

ORIGINAL ARTICLE

Stem Cell-Seeded 3D-Printed Scaffolds Combined with Self-Assembling Peptides for Bone Defect Repair

Haixia Xu, MD,^{1,*} Chengqiang Wang, MD,^{1,*} Chun Liu, MD,^{1,*} Jianjun Li, MD,¹ Ziyue Peng, MD,¹ Jiasong Guo, PhD,¹⁻⁴ and Lixin Zhu, MD¹

Bone defects caused by infection, tumor, trauma, and so on remain difficult to treat clinically. Bone tissue engineering (BTE) has great application prospect in promoting bone defect repair. Polycaprolactone (PCL) is a commonly used material for creating BTE scaffolds. In addition, self-assembling peptides (SAPs) can function as the extracellular matrix and promote osteogenesis and angiogenesis. In the work, a PCL scaffold was constructed by 3D printing, then integrated with bone marrow mesenchymal stem cells (BMSCs) and SAPs. The research aimed to assess the bone repair ability of PCL/BMSC/SAP implants. BMSC proliferation in PCL/SAP scaffolds was assessed via Cell Counting Kit-8. *In vitro* osteogenesis of BMSCs cultured in PCL/SAP scaffolds was assessed by alkaline phosphatase staining and activity assays. Enzyme-linked immunosorbent assays were also performed to detect the levels of osteogenic factors. The effects of BMSC-conditioned medium from 3D culture systems on the migration and angiogenesis of human umbilical vein endothelial cells (HUVECs) were assessed by scratch, transwell, and tube formation assays. After 8 weeks of *in vivo* transplantation, radiography and histology were used to evaluate bone regeneration, and immunohistochemistry staining was utilized to detect neovascularization. *In vitro* results demonstrated that PCL/SAP scaffolds promoted BMSC proliferation and osteogenesis compared to PCL scaffolds, and the PCL/BMSC/SAP conditional medium (CM) enhanced HUVEC migration and angiogenesis compared to the PCL/BMSC CM. *In vivo* results showed that, compared to the blank control, PCL, and PCL/BMSC groups, the PCL/BMSC/SAP group had significantly increased bone and blood vessel formation. Thus, the combination of BMSC-seeded 3D-printed PCL and SAPs can be an effective approach for treating bone defects.

Keywords: self-assembling peptides, bone marrow mesenchymal stem cells, 3D printing, polycaprolactone, osteogenesis, angiogenesis

Impact Statement

Both polycaprolactone (PCL) and self-assembling peptides (SAPs) have been broadly applied in bone defect repair. However, the poor osteoinductivity of PCL and weak mechanical strength of SAPs have limited their clinical application. Here, a 3D-printed PCL scaffold was fabricated for seeding bone marrow mesenchymal stem cells (BMSCs), then combined with SAPs to construct a composite PCL/BMSC/SAP implant for treating the calvarial defect. We showed that transplantation of PCL/BMSC/SAP composite implants clearly promoted bone regeneration and neovascularization. To our knowledge, this is the first study to treat bone defects by combination of BMSC-seeded 3D-printed PCL and SAPs.

Introduction

CLINICAL THERAPY FOR bone defects is still a great challenge for orthopedic surgeons. Autogenous bone grafting is universally regarded as the gold standard for treating

bone defect.¹ However, various drawbacks, such as donor site morbidity and insufficient supply, have restricted the clinical application of autogenous bone.^{2,3} Although extensively used as the bone graft, allogeneic bone poses the risks of disease transmission and immune rejection.^{4,5} Therefore, it is

¹Department of Spine Surgery, Orthopedic Center, Zhujiang Hospital, Southern Medical University, Guangzhou, China.

²Department of Histology and Embryology, Southern Medical University, Guangzhou, China.

³Key Laboratory of Tissue Construction and Detection of Guangdong Province, Guangzhou, China.

⁴Institute of Bone Biology, Academy of Orthopaedics, Guangzhou, China.

*These authors contributed equally to this work.

necessary to develop substitutes for naturally derived bone grafts. Bone tissue engineering (BTE) has been proved to be a promising approach to bone defect therapy because it avoids the complications related to bone grafts.⁶ Biological scaffolds and seeding cells are two important aspects of BTE in repairing bone defects.⁷

Conventional technologies used to fabricate BTE scaffolds mainly involve lyophilization,⁸ gas foaming,⁹ solvent casting, and particulate leaching,¹⁰ but they cannot control exactly the shape and inner structure of the scaffolds. However, the 3D printing technology offers advantages in scaffold customization.¹¹ Three-dimensional-printed scaffolds can perfectly fill the bone defect sites and also provide the desired architecture for bone regeneration and vascularization. Polycaprolactone (PCL) is an FDA-approved synthetic polymer that is nontoxic, has outstanding biocompatibility and biodegradability, and has a low melting point and glass transition temperature.¹² Thus, PCL has been widely utilized in developing 3D-printed scaffolds for bone defect repair.^{12–14} However, the poor osteoinductivity of PCL has limited its use in BTE.¹⁵

As a type of biomaterial consisting of alternating hydrophobic and hydrophilic residues, self-assembling peptides (SAPs) can self-assemble into a 3D interweaving nanofiber scaffold in physiological solutions.¹⁶ SAPs can mimic the natural extracellular matrix (ECM) due to their similarity in structure and function. The nanofiber network of SAPs favors cell–ECM and cell–cell interactions. SAPs have been proved to effectively accelerate cell growth, migration, and differentiation.^{17–19} In addition, SAPs have a lower risk of spreading biological pathogens when compared to animal-derived materials.²⁰ Therefore, SAPs have been broadly used in tissue regeneration, such as reconstruction of injured nerve, liver, and cartilage tissues.^{21–23} SAPs also have been successfully applied in BTE for bone defect therapy. In one study, *in situ* injection of SAPs facilitated functional bone regeneration, which illustrated the favorable osteoconduc-

tive ability of SAPs.²⁴ However, an important drawback of SAPs is their poor mechanical strength, which can cause the structure to break under mechanical stress.¹⁷

The co-transplantation of tissue-engineered bone and SAPs has been an effective strategy for bone defect repair. For example, Li *et al.* prepared SAP-modified demineralized bone matrix (DBM) and verified its effective osteogenesis and bone repair abilities.²⁵ However, whether the combination of 3D-printed scaffolds and SAPs can be an effective tissue engineering scaffold for repairing bone defects is still unknown. In this work, a PCL scaffold was developed by 3D printing technology and seeded with bone marrow mesenchymal stem cells (BMSCs). Then, we integrated PCL/BMSCs with SAPs to construct a composite PCL/BMSC/SAP implant. We hypothesized that the composite implant would promote bone defect repair due to its excellent osteoinductive and pro-angiogenic properties. The schematic illustration of this study is depicted in Figure 1. To test our hypothesis, we assessed the following questions: (1) whether SAPs promote the proliferation and osteogenesis of BMSCs seeded in PCL scaffolds; (2) whether PCL/BMSC/SAP better promotes angiogenesis compared with PCL/BMSC; and (3) whether PCL/BMSC/SAP composite implants accelerate bone defect repair by enhancing osteogenesis and angiogenesis when compared with blank control, PCL, and PCL/BMSC groups.

Materials and Methods

BMSC isolation and culture

This study was approved by the Ethics Institutional Review Board of Zhujiang Hospital of Southern Medical University. BMSCs were obtained and characterized as previously described.²⁶ Newly born New Zealand rabbits were anesthetized to gain their bone marrow of iliac crest (5 mL). Aspirated bone marrow was double diluted in phosphate-buffered saline (PBS; HyClone). Ficoll-Isopaque Plus (Solarbio, China) was overlaid with an equal volume

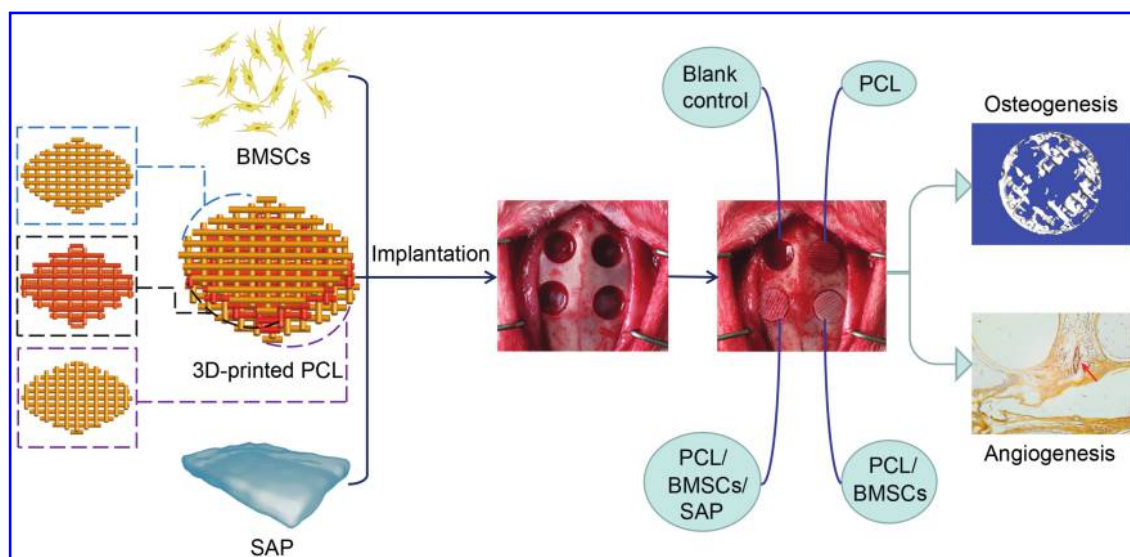


FIG. 1. Schematic illustration of the PCL/BMSC/SAP composite implant, calvarial defect model, transplantation process, and evaluation of the bone repair. The *arrow* showed the blood vessel. BMSC, bone marrow mesenchymal stem cell; PCL, polycaprolactone; SAP, self-assembling peptide. Color images are available online.

of diluted bone marrow to perform density gradient centrifugation (30 min, 2000 rpm). Then, bone marrow mononuclear cells were obtained and resuspended in Dulbecco's modified Eagle's medium (DMEM; Gibco) that contained 1% penicillin/streptomycin (HyClone) and 10% fetal bovine serum (FBS; Gibco). Finally, the cells were cultured at 37°C in a 5% CO₂ incubator. After 48 h, the culture medium was changed to discard the nonadherent cells. During cell culture, the medium was changed every 3 days. When BMSCs reached 80–90% confluence, they were trypsinized with 0.25% trypsin (Gibco) and subcultured ($1 \times 10^4/\text{cm}^2$). BMSCs at passages 3–5 were used for subsequent assays.

Multi-lineage differentiation potential of BMSCs

Multi-lineage differentiation ability of BMSCs was confirmed by the osteogenic and adipogenic induction. For osteogenic induction, cells were cultured in DMEM containing 1% penicillin/streptomycin, 10% FBS, 50 µg/mL ascorbic acid (Sigma), 10 mM β-glycerophosphate (Sigma), and 10 nM dexamethasone (Sigma). After 3 weeks of culture, stainings for alkaline phosphatase (ALP) and alizarin red S were performed to assess their osteogenesis ability.

To assess adipogenic differentiation, cells were cultured in DMEM containing 1% penicillin/streptomycin, 10% FBS, 100 mM indomethacin (Sigma), 10 µg/mL insulin (Sigma), 1 mM dexamethasone, and 0.5 mM 1-methyl-3-isobutylxanthine (Sigma). After 3 weeks of culture, oil red O staining was used to evaluate their adipogenesis ability.

Flow cytometric analysis

Flow cytometry was performed to characterize BMSC immunophenotype. Cells were incubated with mouse monoclonal antibodies against rabbit CD44 (Genetex), CD90 (Abcam, United Kingdom), CD29 (Sigma), CD45 (Genetex), and CD34 (Genetex). The cells then were washed with PBS and incubated with rat anti-mouse IgG secondary antibodies (BD) conjugated with phycoerythrin, FITC, or BD Horizon™ V450. Cell phenotypes were analyzed by a multi-parameter flow cytometer (FACSVerse; BD).

Fabrication of 3D-printed PCL scaffold

PCL (MW = 6W; Meilunbio, China) was used to fabricate 3D-printed scaffolds with a seven-layer structure using a 3D printer (Recongene, China). Printed PCL scaffold was cylindrical (6 mm diameter, 2.1 mm height) with two different porosities: the upper two layers and lower two layers were 25% porous, and the middle three layers were 50% porous. The average porosity of the scaffold was about 35%. Porosities of the scaffold were similar to those of porosities of the human calvaria, including the outer table, inner table, and middle diploe. All scaffolds were soaked in 75% ethanol for 48 h for disinfection and washed twice with PBS before use.

Mechanical test

To assess the mechanical strength of printed PCL scaffolds, a mechanical testing machine (CMT6103; MTS) was used to detect the compressive modulus. The test was performed at a cross-head speed of 1 mm/min. The initial linear region of the stress–strain curve was used to calculate the

compressive modulus. Three-dimensional printed PCL scaffolds with homogeneous porosities of 25%, 35%, and 50% were used as control groups.

Preparation of PCL/BMSC/SAP composite materials

All PCL scaffolds were coated with fibronectin (2 µg/mL; Sigma) at 37°C for 60 min to increase their hydrophilicity and cell adhesion ability before *in vitro* and *in vivo* assays. RADA16-I (1% w/v, PuraMatrix™; Corning), a type of SAP, was used to prepare PCL/BMSC/SAP composite materials. Briefly, BMSCs were seeded in PCL scaffolds and incubated in 96-well culture plates for 24 h. Then, the culture medium was discarded and 20 µL of SAPs were added into the culture plates. Finally, the culture plates were placed at 37°C for 30 min so that SAPs could self-assemble and integrate with PCL/BMSCs.

Scanning electron microscopy

The PCL pore size and adherent cells were observed by scanning electron microscopy (SEM; Hitachi S-3000N, Japan). PCL samples were gold-coated before SEM analysis. To observe adherent cells, the materials were fixed in 2.5% glutaraldehyde at 4°C for 2 h, then dehydrated with serial dilutions (30%, 50%, 70%, 80%, 90%, 95%, 100%, and 100%) of ethanol for 5 min in each concentration. After dehydration, amyl acetate was used to replace the ethanol. The cell-loaded scaffolds then were lyophilized, gold coated, and photographed.

Cell proliferation assays

The proliferation of BMSCs cultured in PCL/SAP scaffolds was detected with Cell Counting Kit-8 (CCK-8; Dojindo, Japan). Briefly, 1×10^4 cells were seeded in PCL scaffolds and cultured in 96-well plates for 24 h. SAPs then were added into the scaffold and cultured for 7 days. Scaffolds without SAPs served as the control group. On days 1, 3, 5, and 7, each well was added with 10 µL of CCK-8 solution, and the sample was incubated at 37°C for 1 h. The optical density values were measured at 450 nm on a spectrophotometer (BioTek). On day 7, cells in both the PCL/BMSC and PCL/BMSC/SAP groups were labeled with Hoechst and Calcein AM stains, and the cell density was measured with a confocal laser scanning microscope (Leica, Wetzlar, Germany).

ALP staining and activity assays

To perform ALP staining, the samples were incubated with 5-bromo-4-chloro-3-indolyl phosphate/nitro blue tetrazolium chloride solution (Beyotime, China) after 14 days of culture in the osteogenic medium. The ALP activity was assessed by colorimetric assay using the ALP Activity Detection Kit (Beyotime). Quantification of p-nitrophenol, an ALP substrate, was measured at 405 nm by a spectrophotometer (BioTek). Total protein level was detected by bicinchoninic acid protein assay kit (Beyotime) and used to normalize ALP activities.

Enzyme-linked immunosorbent assay

After 7 and 14 days of osteoinduction, the supernatant was separately collected from the PCL/BMSC and PCL/

BMSC/SAP culture systems. The concentrations of Runx2, bone morphogenetic protein (BMP)-2, osteocalcin (OCN), and insulin-like growth factor 1 (IGF-1) were detected using corresponding enzyme-linked immunosorbent assay (ELISA) kits (Meimian, China).

Scratch assay

The scratch assay was used to detect the migration of human umbilical vein endothelial cells (HUVECs; ATCC). HUVECs were seeded in 6-well plates (5×10^5 cells/well), and a 200 μ L pipette tip was used to make a linear scratch. The cells were washed twice with PBS and cultured in PCL/BMSC or PCL/BMSC/SAP conditional media (CM). At 0 and 24 h, the scratch and surrounding cells were imaged under a light microscope (Leica). The percentage of scratch healing was analyzed using ImageJ software.

Transwell assay

Transwell chambers (8 μ m, 24-well plates) were also used to perform cell migration assays. PCL/BMSC CM or PCL/BMSC/SAP CM was added into the lower chamber. HUVECs (1×10^5) in serum-free DMEM were added into the upper chamber. After 24 h of incubation, the membranes were cut and stained with crystal violet solution (Solarbio). A cotton swab was used to remove cells on the upper side of the membrane. HUVECs migrated to the lower side of the membrane were counted under a light microscope (Leica).

Tube formation assay

HUVECs were resuspended in PCL/BMSC CM or PCL/BMSC/SAP CM and seeded onto matrigel (BD)-coated 12-well plates (8×10^4 cells/well). The cells were incubated at 37°C for 8 h. Tube-like structures were observed and photographed by inverted microscopy (Leica).

Animal model and surgical procedure

All animal experiments were approved and conducted following the Animal Care and Use Committee of Southern Medical University. Sixteen female New Zealand white rabbits (3 kg on average) were intravenously anesthetized with pentobarbital sodium (3%, 1 mL/kg). A 4 cm linear incision was made from the nasal bone to the midsagittal crest, and the periosteum was carefully dissected from the bone. Four 6 mm diameter calvarial defects (about 2 mm depth) were created with a trephine bur. The upper left defect was left as an empty hole, and the PCL, PCL/BMSC, and PCL/BMSC/SAP were placed in the upper right, lower left, and lower right defects, respectively. The incision then was sutured.

Radiological analysis

The animals were sacrificed by venous air embolism under anesthesia and all calvaria samples were harvested at 8 weeks postsurgery. The samples were analyzed using micro-computed tomography (micro-CT; ZKKS-MCT-Sharp, China) scanning. The detection parameters were set at 70 kV, 100 μ A, and 9 μ m voxel resolution. Three-dimensional images were reconstructed for each bone defect region. Bone mineral density (BMD) and bone volume/total volume (BV/TV) were analyzed using a professional software (ZKKS-MicroCT4.1).

Histological and immunohistochemical analysis

After micro-CT evaluation, samples were fixed in 4% paraformaldehyde for 2 days and decalcified with 10% ethylenediamine tetraacetic acid (Solarbio) for 2 months at room temperature. The decalcified samples were dehydrated in graded ethanol and embedded in paraffin. Slices with 5 μ m thickness were cut coronally from the middle of the implants. Hematoxylin–eosin (HE) and CD31 immunohistochemistry stainings were performed to observe the newly formed bone and vessels. Images were recorded with a camera under a light microscope (Leica).

Statistical analysis

All data were compared using SPSS 24.0 software and presented in the form of mean \pm standard error of the mean. Student's *t*-test was performed to show the differences between two groups and one-way ANOVA analysis was used for comparing multiple groups. $p < 0.05$ was regarded as statistically significant.

Results

Identification of BMSCs

BMSCs were identified by cell morphology, multi-lineage differentiation ability, and surface markers. The cells showed a fibroblast-like morphology (Fig. 1A). After incubation with osteoinduction medium for 3 weeks, BMSCs showed positive staining for ALP and alizarin red S (Fig. 2B, C). After 3 weeks of adipogenic induction, BMSCs were positively stained by oil red O (Fig. 2D). Results of flow cytometry showed that BMSCs expressed CD90, CD44, and CD29, but not CD45 and CD34 (Fig. 2E).

Structure, mechanical strength, and cell adhesion of the PCL scaffold

The PCL scaffold (6 mm diameter, 2.1 mm height) was tablet-like (Fig. 3A). The seven-layer structure of the PCL scaffold was scanned by SEM (Fig. 3B). The upper two and lower two layers were used to mimic the inner and outer cortical tables of the calvaria, and the middle three layers were used to mimic the cranial diploe. In addition, separate cortical and cancellous sections were printed to observe their morphology (Fig. 3C). The porosity difference between cortical and cancellous sections was determined by SEM (Fig. 3D, E). Mechanical test results revealed the compressive modulus increased with the decrease of PCL porosity, and our calvaria-like PCL scaffold with the inhomogeneous porosity (average of 35%) had a better mechanical property than the PCL scaffold with a homogeneous porosity of 35% (Fig. 3F, G). BMSCs seeded in PCL scaffolds were clearly observed by SEM and showed a normal flattened morphology (Fig. 3H).

SAPs promoted the proliferation of BMSCs seeded in PCL scaffolds

To investigate the effect of SAPs on BMSC proliferation, 3D PCL/BMSC and PCL/BMSC/SAP culture systems were established, and CCK-8 assay was performed to evaluate the BMSC proliferation. Cell proliferation rate in the PCL/BMSC/SAP culture system was higher than that in the

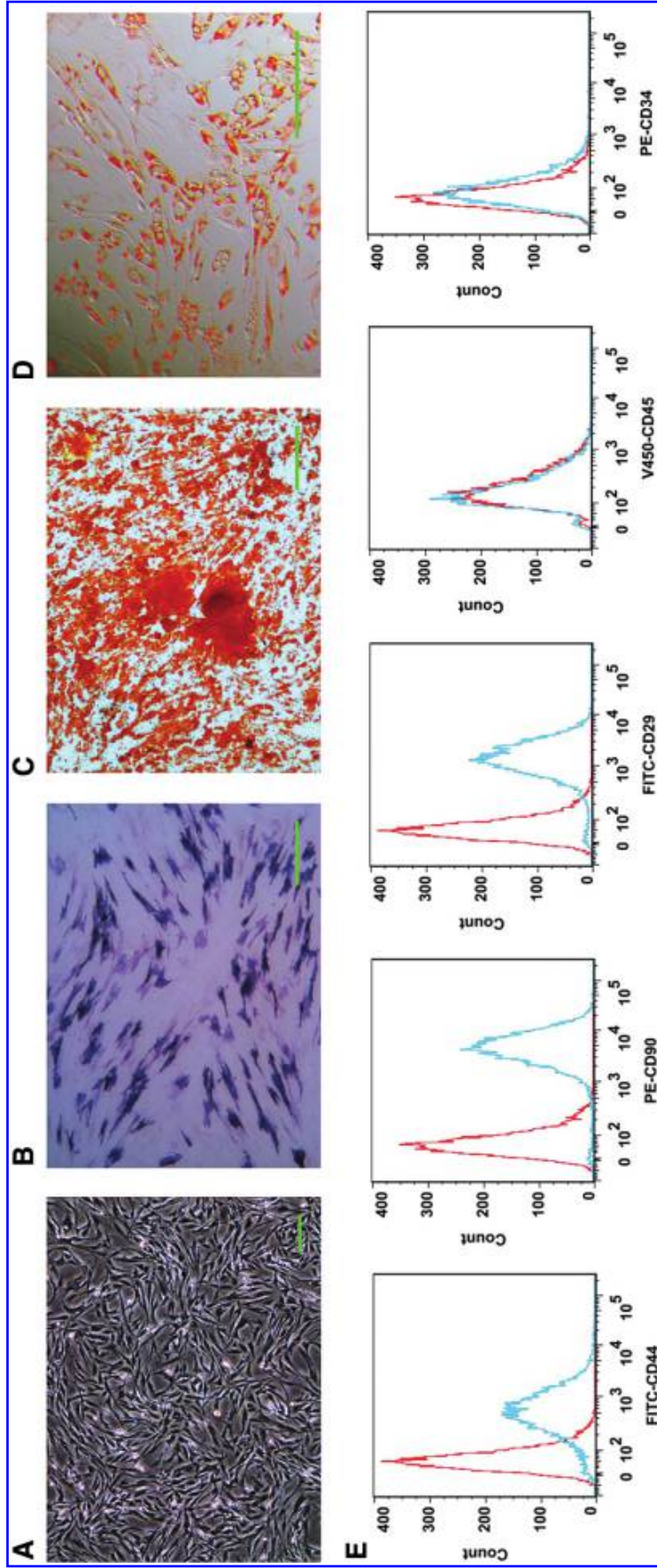


FIG. 2. Identification of rabbit BMSCs. (A) Isolated and cultured BMSCs showed a spindle-shaped morphology. (B) Osteogenic differentiation of BMSCs was assessed by ALP staining. (C) Calcium deposits were detected by Alizarin red S staining. (D) Adipogenic differentiation of BMSCs was assessed by Oil red O staining. (E) Flow cytometry analysis of the expression of CD44, CD90, CD29, CD45, and CD34. Scale bars in (A–D) = 100 μ m. ALP, alkaline phosphatase. Color images are available online.

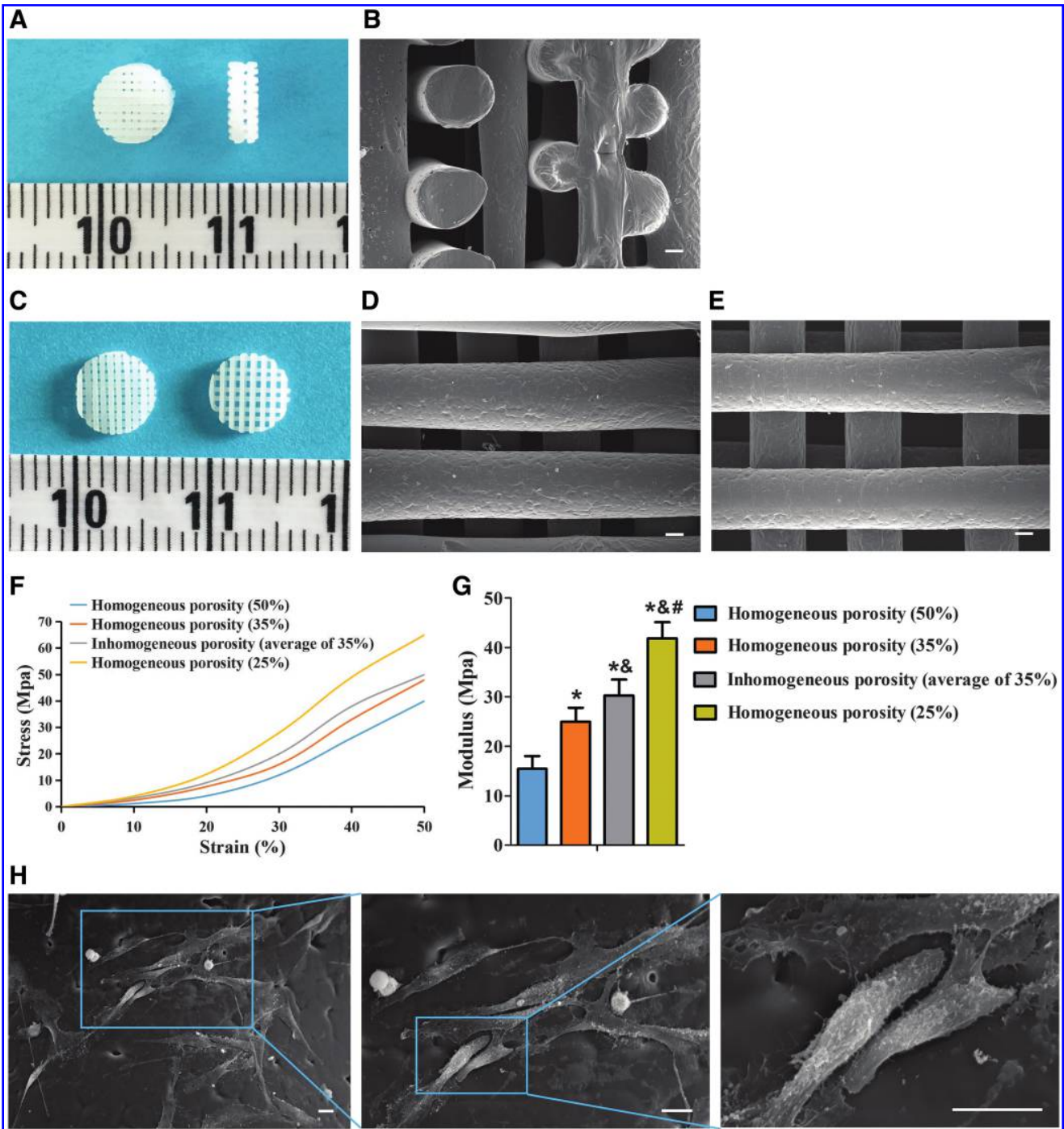


FIG. 3. Structure, mechanical strength, and cell adhesion of the PCL scaffold. **(A)** The morphology of the 3D-printed PCL scaffold. **(B)** The seven-layer structure of the PCL scaffold observed by SEM. **(C)** The morphology of cortical and cancellous sections of the 3D-printed PCL scaffold. **(D)** The morphology of the cortical section observed by SEM. **(E)** The morphology of the cancellous section observed by SEM. Strain–stress curves **(F)** and compressive modulus **(G)** of 3D-printed PCL scaffolds with different structures. **(H)** BMSCs adhered in PCL scaffold were observed under SEM. Scale bars = 100 μm . * p , 0.01 vs homogeneous porosity (50%); & p , 0.01 vs homogeneous porosity (35%); # p , 0.01 vs inhomogeneous porosity (35%). SEM, scanning electron microscopy. Color images are available online.

PCL/BMSC culture system (Fig. 4A). After 7 days of culture, BMSC density in two culture systems was observed by fluorescent staining. The cell density was much higher in the PCL/BMSC/SAP group than in the PCL/BMSC group (Fig. 4B). The results indicated SAPs can promote BMSC proliferation in 3D PCL scaffolds.

SAPs promoted osteogenic differentiation of BMSCs seeded in PCL scaffolds

ALP staining, ALP activity assay, and ELISA were used to detect the cell osteogenic differentiation in PCL/BMSC and PCL/BMSC/SAP culture systems. The ALP staining

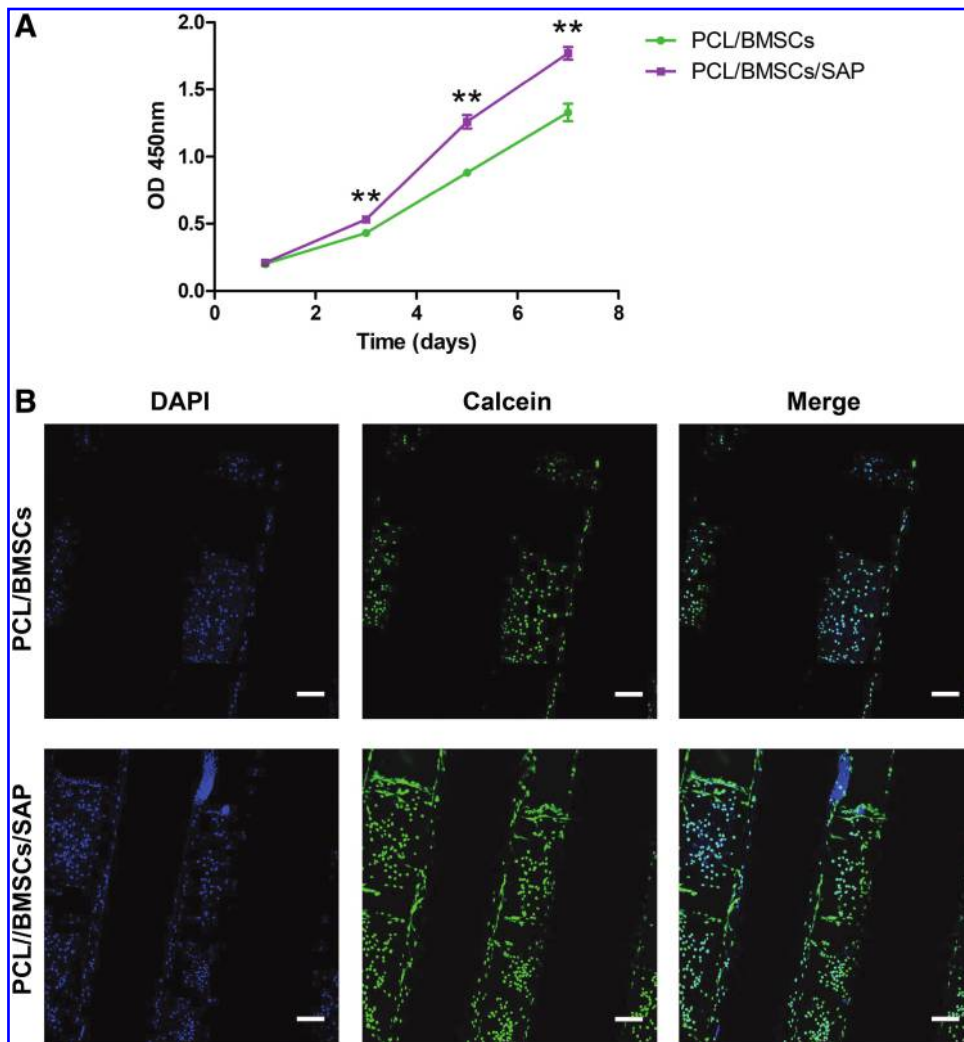


FIG. 4. Proliferation of BMSCs seeded in PCL and PCL/SAP scaffolds. **(A)** Comparison of cell proliferation activity between PCL/BMSC and PCL/BMSC/SAP groups. **(B)** Cell density in PCL/BMSC and PCL/BMSC/SAP groups after 7 days of culture. Scale bars = 100 μm . ** $p < 0.01$. Color images are available online.

results showed that cells in the PCL/BMSC/SAP group displayed a much deeper coloration than that of the PCL/BMSC group after 14 days of culture in osteogenic medium (Fig. 5A, B). The ALP activity assay showed that the PCL/BMSC/SAP group exhibited a higher expression of ALP compared to the PCL/BMSC group (Fig. 5C). The ELISA results showed that the PCL/BMSC/SAP group expressed higher concentrations of Runx2, OCN, BMP-2, and IGF-1 compared to the PCL/BMSC group (Fig. 5D). The results showed SAPs can promote BMSC osteogenesis in a 3D culture system.

PCL/BMSC/SAP CM promoted HUVEC migration and angiogenesis

Scratch and transwell assays were conducted to detect the migration of HUVECs. The scratch assay result showed that more cells migrated toward the wound in the PCL/BMSC/SAP CM group than in the PCL/BMSC CM group after 24 h of incubation (Fig. 6A, B), which indicated that PCL/BMSC/SAP composites can promote cell migration and wound healing. The transwell assay result showed that PCL/BMSC/SAP CM drove more cells across the membrane than PCL/BMSC CM, which also indicated that PCL/BMSC/SAP composites can promote the migration of HUVECs

(Fig. 6C, D). Tube formation assay was performed to detect the angiogenesis of HUVECs under PCL/BMSC/SAP CM or PCL/BMSC CM. PCL/BMSC/SAP CM resulted in a larger number of tube-like structures than PCL/BMSC CM (Fig. 6E, F). Thus, the PCL/BMSC/SAP composite is superior to the PCL/BMSC composite in promoting angiogenesis.

PCL/BMSC/SAP composite implants promoted repair of rabbit calvarial defect

Radiology and histology were used to assess the bone defect repair ability of PCL/BMSC/SAP implants. Micro-CT was performed to assess bone regeneration. The control group showed a minimum level of mineralization, the PCL group displayed moderate mineralization, and the bone healing of the PCL/BMSC group was better than that of the control and PCL groups (Fig. 7A). However, the PCL/BMSC/SAP group had the largest amount of mineralized tissue among all four groups (Fig. 7A). The new bone in each group was quantified based on BMD and BV/TV, which are important trabecular parameters. The BMD and BV/TV of the PCL/BMSC/SAP group were much higher than those of the control, PCL, and PCL/BMSC groups (Fig. 7B, C).

HE and CD31 immunohistochemistry stainings were performed to evaluate bone formation and neovascularization.

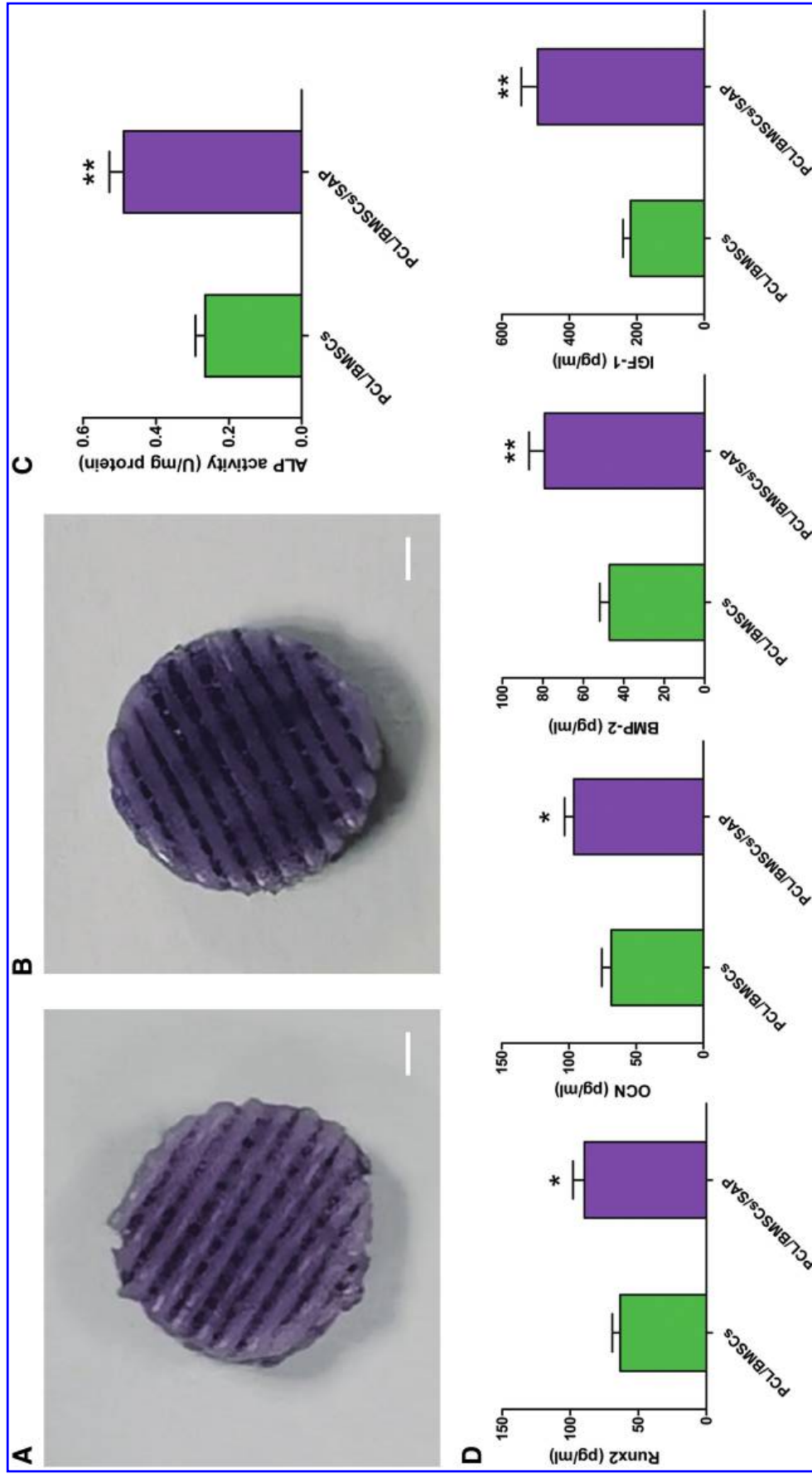


FIG. 5. Osteogenic differentiation of BMSCs seeded in PCL and PCL/SAP scaffolds. **(A)** ALP staining of BMSCs cultured in PCL scaffold. **(B)** ALP staining of BMSCs cultured in PCL/SAP scaffold. **(C)** ALP activity assay after 7 days of osteogenic induction. **(D)** Secretion of osteogenic factors in PCL/BMSC and PCL/BMSC/SAP groups. Scale bars = 1 mm. * $p < 0.05$, ** $p < 0.01$. Color images are available online.

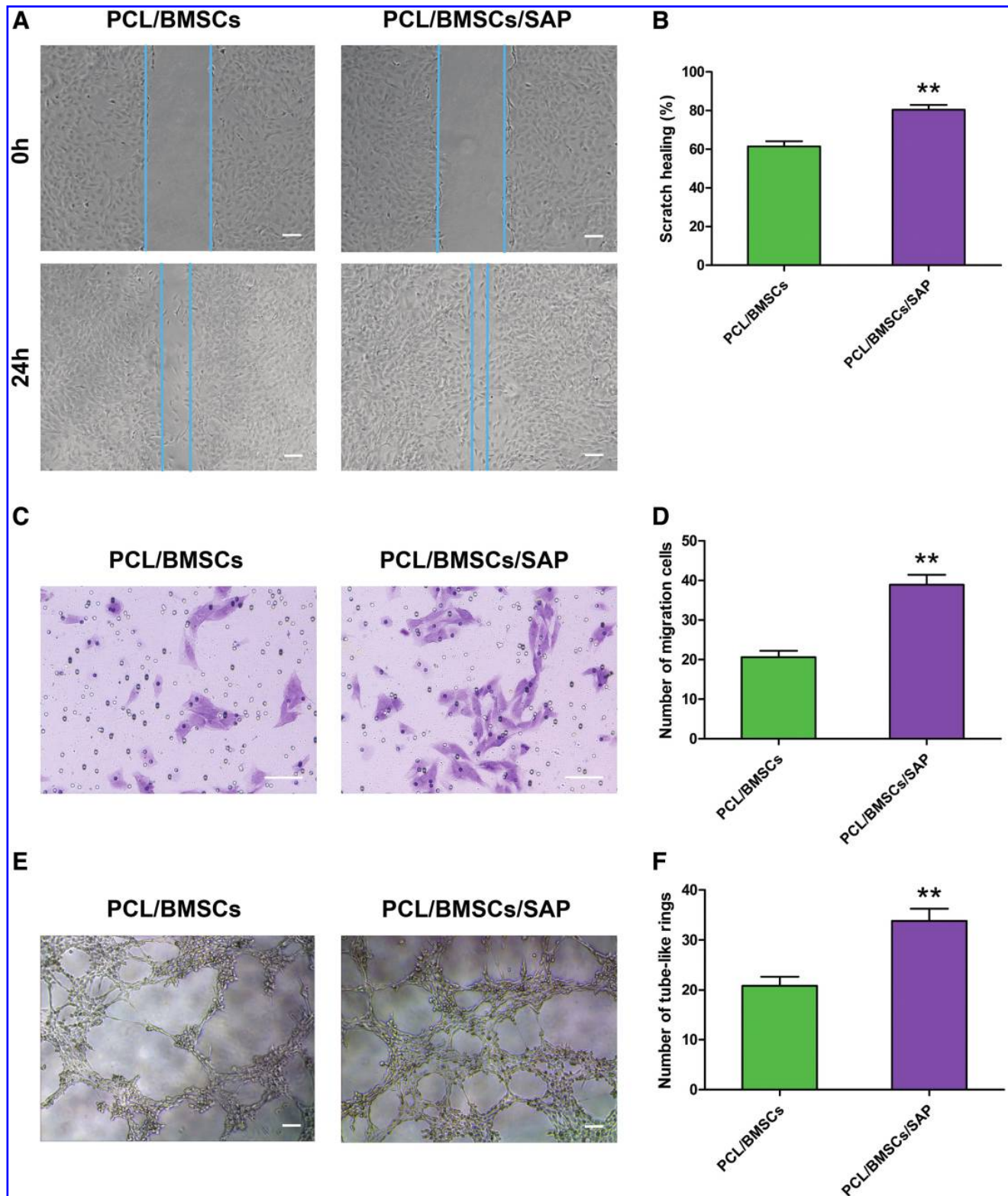


FIG. 6. Migration and angiogenesis of HUVECs cultured in PCL/BMSC and PCL/BMSC/SAP CM. **(A)** HUVEC migration evaluated by scratch assay. **(B)** Percentage of scratch healing in both groups. **(C)** HUVEC migration assessed by transwell assay. **(D)** Number of migration cells in both groups. **(E)** HUVEC angiogenesis assessed by tube formation assay. **(F)** Quantitative analysis of number of tube-like structures. Scale bars=100 μ m. ****** p <0.01. CM, conditional medium; HUVEC, human umbilical vein endothelial cell. Color images are available online.

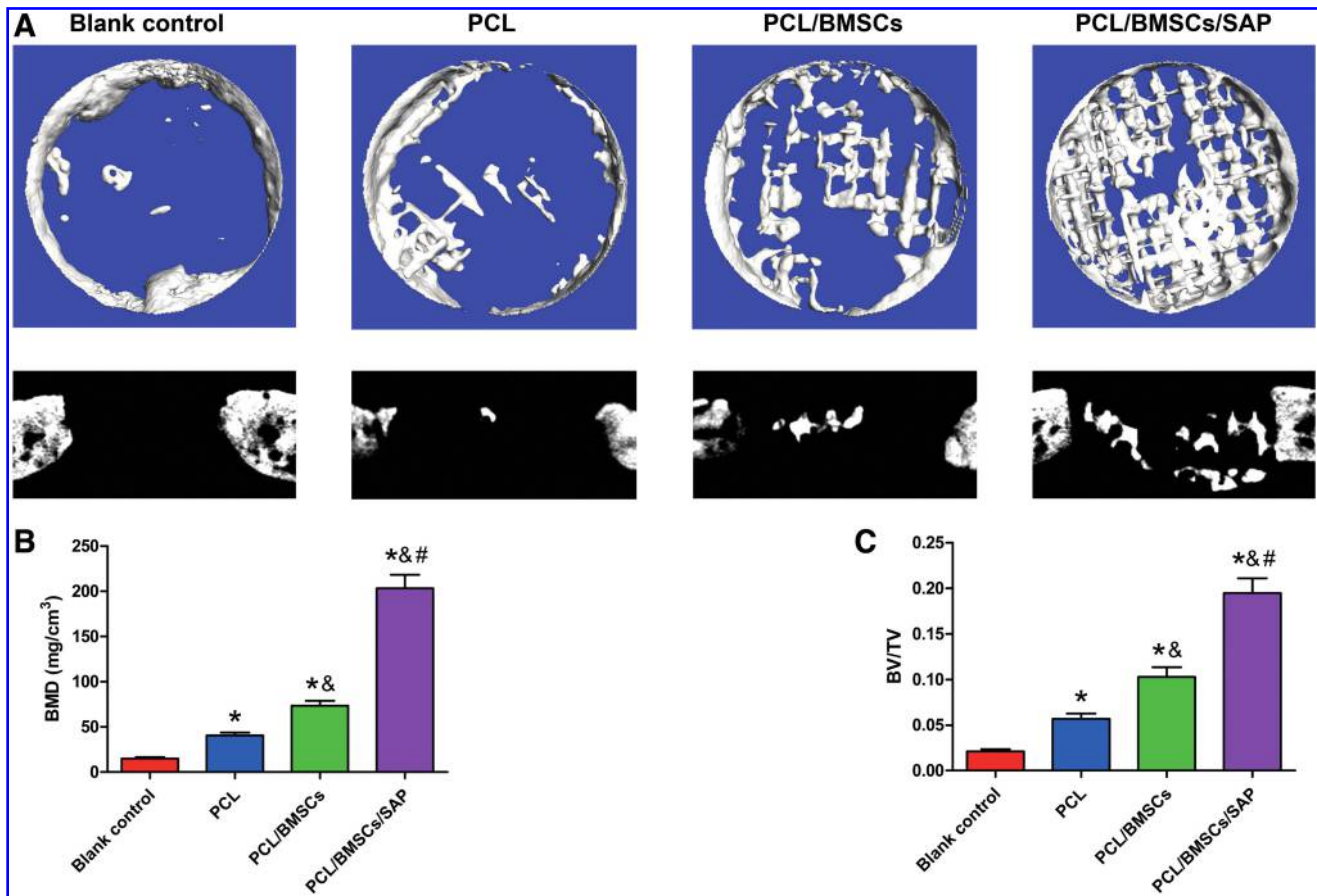


FIG. 7. Repair of rabbit calvarial defect in each group by radiologic evaluation. (A) Three-dimensional and 2D micro-CT images of the calvarial defect region in each group. (B) Quantitative analysis of the trabecular bone parameter (BMD) based on reconstructed 3D images showed in Figure 6A. (C) Quantitative analysis of another trabecular bone parameter (BV/TV) based on images showed in Figure 6A. Significance compared to blank control group (*), PCL group (&), and PCL/BMSC group (#). BMD, bone mineral density; BV/TV, bone volume/total volume, micro-CT, micro-computed tomography. Color images are available online.

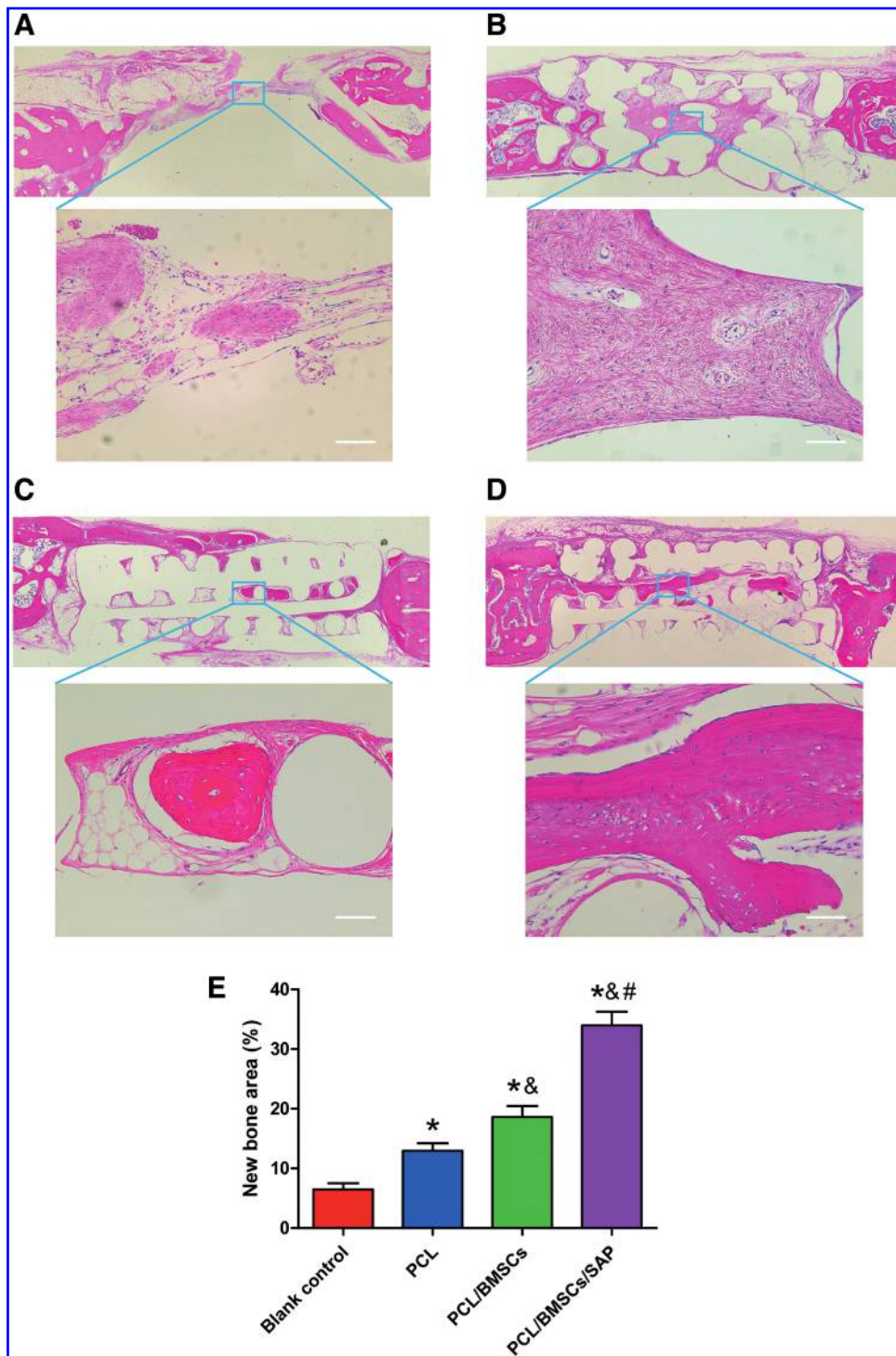
The HE staining results showed that more new bone formation occurred in the PCL/BMSC/SAP group when compared to the other three groups (Fig. 8). Moreover, the center of the bone defect was occupied by fibrous tissue in both the control and PCL groups; bone tissue was observed at the center of the bone defect in the PCL/BMSC group; and much more new bone was present at the defect center in the PCL/BMSC/SAP group (Fig. 8). The CD31 immunohistochemistry staining results also showed that higher blood vessel density was present in the PCL/BMSC/SAP group compared to other three groups (Fig. 9). These results demonstrated that PCL/BMSC/SAP composite implants can promote bone regeneration and neovascularization.

Discussion

Suitable porosity of implanted scaffolds is of vital importance for bone defect repair. Scaffolds with higher porosity tend to have a poorer mechanical property and fewer adhered seeding cells, and lower porosity results in insufficient space in scaffolds for cell infiltration and bone regeneration.²⁷ In our study, 3D printing technology was used to fabricate the scaffold for its flexibility in controlling the porosity. The effect of porosity of 3D-printed PCL on bone regeneration has been

investigated previously. Shim *et al.* fabricated 3D-printed PCL scaffolds with different porosities for repairing bone defects and found that the scaffold with 30% porosity had better mechanical strength and osteoconductive properties compared to scaffolds with 50% and 70% porosity.²⁸ In addition, it was reported that the porosities of human cortical bone and trabecular bone are 5–15% and 40–95%, respectively.²⁹ In our study, the PCL scaffold was designed based on its whole and segmental porosities, and we set porosities at 25% in cortical sections and 50% in cancellous section, with an average porosity of 35%. Compared with the PCL scaffold with a homogeneous porosity of 35%, the calvaria-like PCL scaffold showed a better mechanical strength, which indicated that the bionic structure of our PCL scaffold could provide adequate mechanical support for bone regeneration.

Excellent proliferation ability of transplanted cells is important for their application in tissue engineering. SAPs have been shown to promote the proliferation of diverse cell types, such as embryonic fibroblasts and ciliary pigment epithelial cells.^{17,30} Several factors confer their beneficial effects on cell growth. First, the nanofiber structure and over 99% water content of SAPs provide a real 3D microenvironment for cell growth.³¹ Second, the network formed by interweaving nanofibers benefits gas and nutrient diffusion.³²

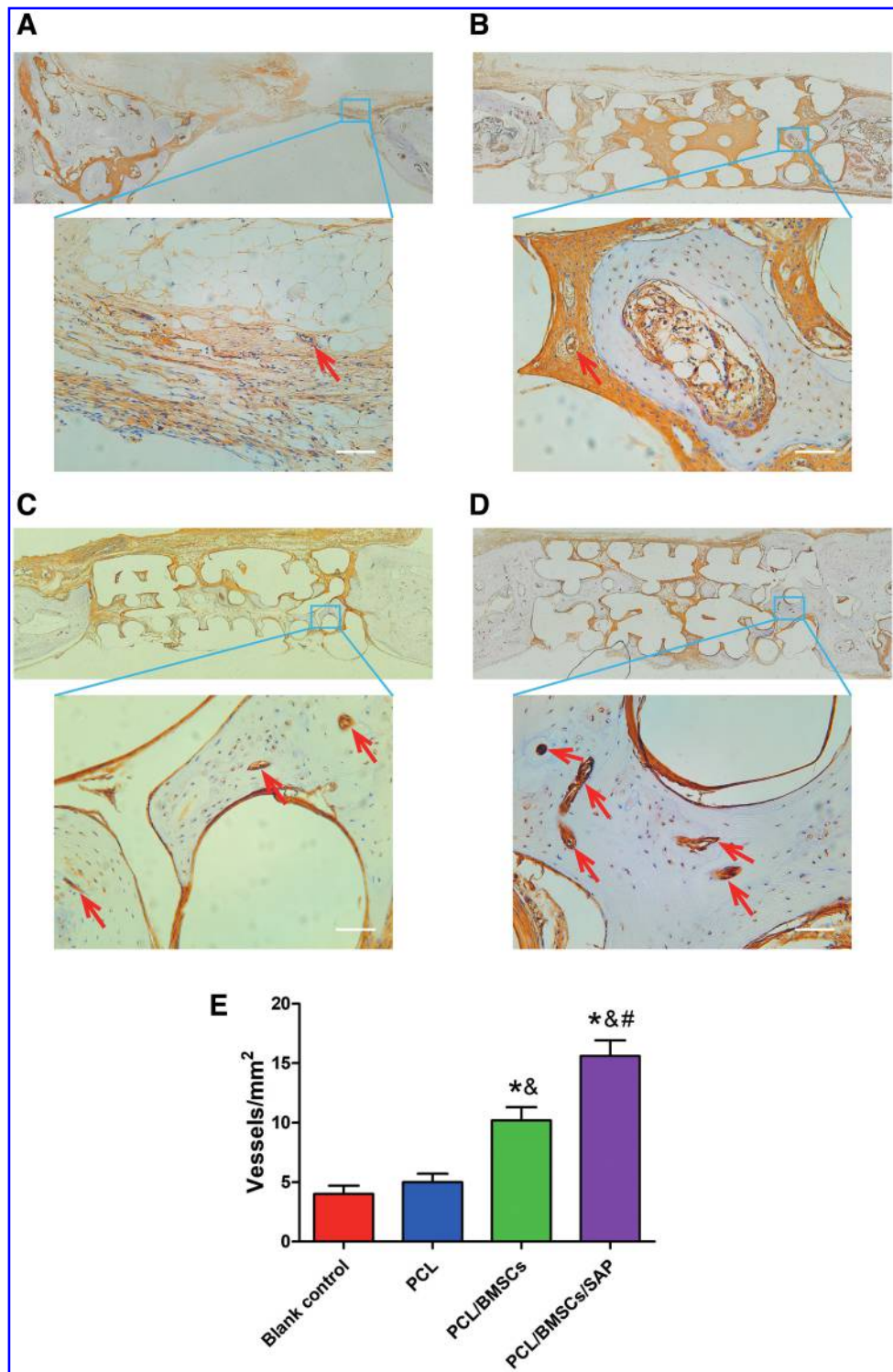


Third, the noncovalent bonds of SAPs such as ionic bonds and hydrogen bonds drive their self-assembling process, and these weak bonds contribute to cell–cell and cell–matrix interactions that can promote cell growth and proliferation.³³

As is known, bone tissue regeneration derives directly from the differentiation of osteogenic stem or progenitor cells. Previous studies reported that the osteogenesis of mesenchymal stem cells (MSCs) could be successfully induced in a 3D cell culture using SAPs.^{19,34} In addition, Li *et al.* reported that DBM/SAP scaffolds can promote more *in vitro*

osteogenesis in comparison with the DBM alone.²⁵ Similar to previous studies, we found that PCL/SAP scaffolds promoted BMSC osteogenic differentiation compared to PCL alone scaffolds. During osteogenic differentiation of BMSCs, SAPs can serve as a vehicle for intercellular interactions and signal transduction.³⁵ SAP-induced osteogenesis may also result from the promoted growth factor-enriching ability. As illustrated by previous studies, the self-assembling network structure and charged residues of SAPs can enrich more factors (e.g., BMP-6 and VEGF) for cell differentiation.^{36,37}

FIG. 9. Neovascularization in the bone defect region of each group evaluated by CD31 immunohistochemistry staining. (A) Blank control group. (B) PCL group. (C) PCL/BMSC group. (D) PCL/BMSC/SAP group. The arrows showed the vessels. (E) The vessel density in the bone defect region of each group. Scale bars = 100 μ m. Significance compared to blank control group (*), PCL group (&), and PCL/BMSC group (#). Color images are available online.



Sufficient angiogenesis is necessary for bone defect repair, and vascularization of tissue engineering implants is a key factor for successful bone regeneration. Migration and angiogenic differentiation of endogenous cells are the main ways by which implant vascularization occurs. It was reported that SAPs showed an ability to recruit endogenous cells into the ischemic site.¹⁸ SAPs can also enhance the endothelialization of biomaterials, which is an important indicator that vascularization in implants has been achieved.³⁸

MSCs seeded in SAPs showed increased expression of pro-angiogenic factors, such as IGF-1 and hepatocyte growth factors.³⁷ In our study, BMSCs in PCL/SAP scaffolds promoted HUVEC migration and angiogenesis via indirect contact, and we believe that this effect resulted from increased BMSC-derived growth factors induced by SAPs.

As an ideal bone filling material, 3D-printed PCL can reconstruct the original shape of defect sites and guide bone ingrowth.³⁹ However, our *in vivo* results showed that

transplantation of PCL alone resulted in only slight bone regeneration, which was indicative of the poor osteoinductive property of PCL. Although PCL/BMSC implants had osteogenesis ability and induced more bone formation than PCL alone, the regenerative bone mass was still unsatisfactory, likely due to inadequate osteogenic and angiogenic properties of the implant. In contrast, PCL/BMSC/SAP implants exhibited better bone defect repair ability. Thus, the *in vivo* results also showed SAPs promoted osteogenesis and angiogenesis. We surmise that two main factors are involved in the biological activity of SAPs. First, SAPs can promote implanted BMSC proliferation and osteogenic differentiation. Second, SAPs can induce endogenous stem cell osteogenic and angiogenic differentiation by enhancing implanted BMSC paracrine activity.

Conclusions

The PCL scaffold and SAPs are promising biomaterials for repairing bone defects. This is the first study to combine BMSC-seeded 3D-printed PCL with SAPs to promote bone defect repair. Results of our study show that individualized PCL scaffolds are easily fabricated using 3D printing technology and that SAPs are an ideal ECM for accelerating osteogenesis and angiogenesis. *In situ* transplantation of PCL/BMSC/SAP composite implants clearly promoted bone regeneration and neovascularization. Thus, the combination of BMSC-seeded 3D PCL scaffold with SAPs may provide an effective strategy for treating bone defects.

Authors' Contributions

H.X.: Conception, methodology, investigation, and writing. C.W.: Conception and writing. C.L.: Methodology and writing. J.L.: Supervision and writing. Z.P.: Methodology and writing. J.G.: Conception and writing. L.Z.: Resources, writing, and supervision.

Acknowledgments

The authors thank the National Natural Science Foundation of China (81974329, 81672140) and the Natural Science Foundation of Guangdong Province (2017A030312009, 2017A030313111) for funding this research. We thank International Science Editing for English editing.

Disclosure Statement

No competing financial interests exist.

Funding Information

This research was funded by the National Natural Science Foundation of China (81974329, 81672140) and the Natural Science Foundation of Guangdong Province (2017A030312009, 2017A030313111).

References

- Baldwin, P., Li, D.J., Auston, D.A., *et al.* Autograft, allograft, and bone graft substitutes: clinical evidence and indications for use in the setting of orthopaedic trauma surgery. *J Orthop Trauma* **33**, 203, 2019.
- Ng, J., Spiller, K., Bernhard, J., *et al.* Biomimetic approaches for bone tissue engineering. *Tissue Eng Part B Rev* **23**, 480, 2017.
- Alluri, R., Song, X., Bougioukli, S., *et al.* Regional gene therapy with 3D printed scaffolds to heal critical sized bone defects in a rat model. *J Biomed Mater Res A* **107**, 2174, 2019.
- Li, X., Feng, Q., Liu, X., *et al.* Collagen-based implants reinforced by chitin fibres in a goat shank bone defect model. *Biomaterials* **27**, 1917, 2006.
- Flierl, M.A., Smith, W.R., Mauffrey, C., *et al.* Outcomes and complication rates of different bone grafting modalities in long bone fracture nonunions: a retrospective cohort study in 182 patients. *J Orthop Surg Res* **8**, 33, 2013.
- Watson, B.M., Vo, T.N., Tataru, A.M., *et al.* Biodegradable, phosphate-containing, dual-gelling macromers for cellular delivery in bone tissue engineering. *Biomaterials* **67**, 286, 2015.
- Lee, J.S., Jin, Y., Park, H.J., *et al.* In situ bone tissue engineering with an endogenous stem cell mobilizer and osteoinductive nanofibrous polymeric scaffolds. *Biotechnol J* **12**, 2017. DOI: 10.1002/biot.201700062.
- Wang, F., Pang, Y., Chen, G., *et al.* Enhanced physical and biological properties of chitosan scaffold by silk proteins cross-linking. *Carbohydr Polym* **229**, 115529, 2020.
- Kim, S.E., and Tiwari, A.P. Three dimensional polycaprolactone/cellulose scaffold containing calcium-based particles: a new platform for bone regeneration. *Carbohydr Polym* **250**, 116880, 2020.
- Mondal, D., Lin, S., Rizkalla, A.S., *et al.* Porous and biodegradable polycaprolactone-borophosphosilicate hybrid scaffolds for osteoblast infiltration and stem cell differentiation. *J Mech Behav Biomed Mater* **92**, 162, 2019.
- Ma, H., Feng, C., Chang, J., *et al.* 3D-printed bioceramic scaffolds: from bone tissue engineering to tumor therapy. *Acta Biomater* **79**, 37, 2018.
- Ji, X., Yuan, X., Ma, L., *et al.* Mesenchymal stem cell-loaded thermosensitive hydroxypropyl chitin hydrogel combined with a three-dimensional-printed poly(epsilon-caprolactone)/nano-hydroxyapatite scaffold to repair bone defects via osteogenesis, angiogenesis and immunomodulation. *Theranostics* **10**, 725, 2020.
- Lee, S.J., Won, J.E., Han, C., *et al.* Development of a three-dimensionally printed scaffold grafted with bone forming peptide-1 for enhanced bone regeneration with in vitro and in vivo evaluations. *J Colloid Interface Sci* **539**, 468, 2019.
- Buyuksungur, S., Endogan Tanir, T., Buyuksungur, A., *et al.* 3D printed poly(epsilon-caprolactone) scaffolds modified with hydroxyapatite and poly(propylene fumarate) and their effects on the healing of rabbit femur defects. *Biomater Sci* **5**, 2144, 2017.
- Nyberg, E., Rindone, A., Dorafshar, A., *et al.* Comparison of 3D-printed poly-e-caprolactone scaffolds functionalized with tricalcium phosphate, hydroxyapatite, bio-oss, or decellularized bone matrix. *Tissue Eng Part A* **23**, 503, 2017.
- Koutsopoulos, S. Self-assembling peptide nanofiber hydrogels in tissue engineering and regenerative medicine: progress, design guidelines, and applications. *J Biomed Mater Res A* **104**, 1002, 2016.
- Dégano, I.R., Quintana, L., Vilalta, M., *et al.* The effect of self-assembling peptide nanofiber scaffolds on mouse embryonic fibroblast implantation and proliferation. *Biomaterials* **30**, 1156, 2009.

18. Park, H.S., Choi, G.H., Kim, D., *et al.* Use of self-assembling peptides to enhance stem cell function for therapeutic angiogenesis. *Stem Cells Int* **2018**, 4162075, 2018.
19. Ozeki, M., Kuroda, S., Kon, K., *et al.* Differentiation of bone marrow stromal cells into osteoblasts in a self-assembling peptide hydrogel: in vitro and in vivo studies. *J Biomater Appl* **25**, 663, 2011.
20. Holmes, T.C. Novel peptide-based biomaterial scaffolds for tissue engineering. *Trends Biotechnol* **20**, 16, 2002.
21. Koutsopoulos, S., and Zhang, S. Long-term three-dimensional neural tissue cultures in functionalized self-assembling peptide hydrogels, matrigel and collagen I. *Acta Biomater* **9**, 5162, 2013.
22. Cheng, T.Y., Wu, H.C., Huang, M.Y., *et al.* Self-assembling functionalized nanopptides for immediate hemostasis and accelerative liver tissue regeneration. *Nanoscale* **5**, 2734, 2013.
23. Lv, X., Sun, C., Hu, B., *et al.* Simultaneous recruitment of stem cells and chondrocytes induced by a functionalized self-assembling peptide hydrogel improves endogenous cartilage regeneration. *Front Cell Dev Biol* **8**, 864, 2020.
24. Misawa, H., Kobayashi, N., Soto-Gutierrez, A., *et al.* PuraMatrix facilitates bone regeneration in bone defects of calvaria in mice. *Cell Transplant* **15**, 903, 2006.
25. Li, Z., Hou, T., Luo, F., *et al.* Bone marrow enriched graft, modified by self-assembly peptide, repairs critically-sized femur defects in goats. *Int Orthop* **38**, 2391, 2014.
26. Fan, L., Zhang, C., Yu, Z., *et al.* Transplantation of hypoxia preconditioned bone marrow mesenchymal stem cells enhances angiogenesis and osteogenesis in rabbit femoral head osteonecrosis. *Bone* **81**, 544, 2015.
27. Loh, Q.L., and Choong, C. Three-dimensional scaffolds for tissue engineering applications: role of porosity and pore size. *Tissue Eng Part B Rev* **19**, 485, 2013.
28. Shim, J.H., Jeong, J.H., Won, J.Y., *et al.* Porosity effect of 3D-printed polycaprolactone membranes on calvarial defect model for guided bone regeneration. *Biomed Mater* **13**, 015014, 2017.
29. Morgan, E.F., Unnikrisnan, G.U., and Hussein, A.I. Bone mechanical properties in healthy and diseased states. *Annu Rev Biomed Eng* **20**, 119, 2018.
30. Jasty, S., Suriyanarayanan, S., and Krishnakumar, S. Influence of self-assembling peptide nanofibre scaffolds on retinal differentiation potential of stem/progenitor cells derived from ciliary pigment epithelial cells. *J Tissue Eng Regen Med* **11**, 509, 2017.
31. Gelain, F., Horii, A., and Zhang, S. Designer self-assembling peptide scaffolds for 3-d tissue cell cultures and regenerative medicine. *Macromol Biosci* **7**, 544, 2007.
32. Lutolf, M.P., Gilbert, P.M., and Blau, H.M. Designing materials to direct stem-cell fate. *Nature* **462**, 433, 2009.
33. Recha-Sancho, L., Moutos, F.T., Abellà, J., *et al.* Dedifferentiated human articular chondrocytes redifferentiate to a cartilage-like tissue phenotype in a poly(epsilon-caprolactone)/self-assembling peptide composite scaffold. *Materials (Basel)* **9**, 472, 2016.
34. Tsukamoto, J., Naruse, K., Nagai, Y., *et al.* Efficacy of a self-assembling peptide hydrogel, SPG-178-Gel, for bone regeneration and three-dimensional osteogenic induction of dental pulp stem cells. *Tissue Eng Part A* **23**, 1394, 2017.
35. Luo, Z., and Zhang, S. Designer nanomaterials using chiral self-assembling peptide systems and their emerging benefit for society. *Chem Soc Rev* **41**, 4736, 2012.
36. Hou, T., Li, Z., Luo, F., *et al.* A composite demineralized bone matrix—self assembling peptide scaffold for enhancing cell and growth factor activity in bone marrow. *Biomaterials* **35**, 5689, 2014.
37. Cai, H., Wu, F.Y., Wang, Q.L., *et al.* Self-assembling peptide modified with QHREDGS as a novel delivery system for mesenchymal stem cell transplantation after myocardial infarction. *FASEB J* **33**, 8306, 2019.
38. Martínez-Ramos, C., Arnal-Pastor, M., Vallés-Lluch, A., *et al.* Peptide gel in a scaffold as a composite matrix for endothelial cells. *J Biomed Mater Res A* **103**, 3293, 2015.
39. Pae, H.C., Kang, J.H., Cha, J.K., *et al.* 3D-printed polycaprolactone scaffold mixed with beta-tricalcium phosphate as a bone regenerative material in rabbit calvarial defects. *J Biomed Mater Res B Appl Biomater* **107**, 1254, 2019.

Address correspondence to:

Jiasong Guo, PhD

Department of Histology and Embryology

Southern Medical University

Guangzhou 510515

China

E-mail: jiasongguo@smu.edu.cn

Lixin Zhu, MD

Department of Spine Surgery

Orthopedic Center

Zhujiang Hospital

Southern Medical University

Guangzhou 510280

China

E-mail: zhulixin1966@163.com

Received: March 13, 2021

Accepted: June 22, 2021

Online Publication Date: December 30, 2021